RESEARCH ARTICLE

Check for updates

Low-cost and multi-level structured NiFeMn alloy@NiFeMn oxyhydroxide electrocatalysts for highly efficient overall water splitting†

Zeyu Ge,[a,b] Fei Wang, [ID][a] Junji Guo,[a] Jungang Ma,[a,b] Chunyan Yu,[c] Aihua Zhong [ID][a,c] and Yizhu Xie [ID] *[a,b,c]

Fabricating energy-saving, inexpensive and high-activity electrocatalysts for overall water splitting has always been a significant challenge. Electrochemical deposition is considered as a promising method for large-scale industrial applications, but it is prone to generating dense compounds, which reduces the effective catalytic activity area of electrodes. Herein, a low-cost and high-performance bifunctional NiFeMn alloy@NiFeMn oxyhydroxide electrocatalyst was deposited by several minute electrodeposition. Due to the doping of manganese, this method effectively engineers a multi-level dendritic NiFeMn alloy and oxyhydroxide layer, and significantly reduces the energy barrier for the oxygen evolution reaction (OER) and hydrogen evolution reaction (HER), which has been proved by the density functional theory calculations. Specifically, the as-prepared catalyst shows excellent electrocatalytic performance for OER (219 mV) and HER (19 mV) at a current density of 10 mA cm^{-2}. Experimentally and theoretically, the catalyst demonstrated extraordinary performance for overall water splitting and provides a new possibility for industrialization in the future.

Introduction

In order to reduce the adverse effects of traditional fossil energy on the environment, it is attractive to obtain oxygen and hydrogen fuel from water electrolysis by using renewable energy sources, such as wind power, hydropower and solar power.[1,2] However, the use of renewable energy to industrialize electrolyzed water still requires a high cost compared to hydrogen, which is generated from the petrochemical industry, this means that there is still a lot of work required for the production of hydrogen from water splitting. Principally, water electrolysis consists of two half-cell reactions, which are OER and HER.[3,4] The OER process is considered to be kinetically sluggish because it includes several proton and electron couple transfer steps.[5] Some precious metal oxide electrocatalysts, such as the oxides of ruthenium and iridium, are identi-

fied to be remarkable OER catalysts, while the exorbitant price and scarcity of these noble metals seriously limit their widespread applications.[6,7] Similar problems are encountered when the platinum-based catalysts are used for HER.[8] Moreover, when the cathode catalyst is different from the anode catalyst, different production processes, equipment and raw materials are needed, which means higher production costs for water splitting.[9] Therefore, it is urgently needed to find earth-abundant, high-efficient and durable catalysts for HER and OER.

Recently, massive efforts have been aimed to research various earth-abundant metal-based electrocatalysts, such as transition-metal chalcogenides, oxides, selenides, borides, nitrides, and phosphides.[10–14] Among the abovementioned catalysts, the NiFe-based oxide and oxyhydroxide electrocatalysts have been researched extensively for their high electrolysis performance in alkaline electrolytes.[15] Some significant research efforts have been devoted to increase the performance of NiFe-based catalysts, such as special morphology construction, surface defect engineering and integration with some conductive materials.[16–18] Specifically, increasing numbers of research studies focus on the construction of active materials by adding new elements to form multi-element catalysts because modulating the energy levels of the catalyst by adding new elements to regulate the electronic structure could change the bond length of the active site and the adsorption energy of the HER/

[a]Shenzhen Key Laboratory of Advanced Thin Films and Applications, College of Physics and Optoelectronic engineering, Shenzhen University, Shenzhen, 518060, China. E-mail: yzxie@szu.edu.cn
[b]College of Materials Science and Engineering, Shenzhen University, Shenzhen, 518060, China
[c]Key Laboratory of Optoelectronic Devices and Systems of Ministry of Education and Guangdong Province, College of Physics and Optoelectronic Engineering, Shenzhen University, Shenzhen 518060, China
†Electronic supplementary information (ESI) available. See DOI: 10.1039/d1qi00215e

This journal is © the Partner Organisations 2021

Inorg. Chem. Front., 2021, **8**, 2713–2724 | **2713**

OER reaction intermediates.[19] For example, NiVFe trimetallic phosphor nitride was synthesized for overall water splitting, which attained a current density of 10 mA cm^{-2} with the overpotentials of 79 mV and 229 mV for HER and OER, respectively.[20] The two-electrode electrolyzer both fabricated by CoFeZr oxides reached 10 mA cm^{-2} at 1.63 V for water electrolysis.[21] However, there are few studies on multi-element catalysts containing Mn because pure manganese-based oxide catalysts are relatively catalytically inert and exhibit inherent poor conductivity.[22] However, manganese plays a crucial role in water oxidation in nature, and it is the third most abundant transition-metal in the earth's crust.[23] In order to imitate the green and efficient method of water splitting in nature and reduce the cost of electrocatalyst materials, substantial work still needs to be done for the synergy of Mn and NiFe-based catalysts to increase the bifunctional electrocatalytic activity.

Many breakthroughs have been made in the synthesis of catalysts for the electrolysis of water, but those electrocatalysts are still far away from large-scale water electrolysis. Since many complex chemical or physical methods were used to fabricate the catalysts in order to achieve a better performance than that of the current industrial catalysts, it significantly increases the cost of water splitting.[24,25] Additionally, most of the catalysts are in the form of a powder of nanoparticles or nanosheets. A binder will inevitably be used when coating the powders onto the electrode, which will lead to a decrease in conductivity and reduced catalytically active sites.[26,27] Although many catalysts are also directly synthesized onto the substrate, their electrochemically active surface area (ECSA) is often subjected to the small surface area of the substrates.[28] These factors limit further improvement of the catalyst performance. Meanwhile, the mechanisms among the multiple elements of transition metal catalysts are still not fully mastered. Thus, an in-depth research study on achieving low-cost and high-performance of multi-component catalysts is urgently needed.

Herein, we successfully fabricated NiFeMn alloy (core)–oxyhydroxide nanosheet (shell) arrays (denoted as NiFeMn-AOs) as high-performance bifunctional catalysts for both OER and HER. The NiFeMn-AOs was fabricated on nickel foam (NF) or carbon cloth substrate by chronoamperometry deposition method. The NiFeMn-AOs is cheaper and more environmentally friendly compared with the NiFe-based catalysts synthesized through conventional hydrothermal method or physical vapor deposition method. The particular multi-level dendritic structures of the NiFeMn-AOs samples, which possess larger ECSA and more active sites, facilitate faster electron and ion transfer. As a result, the as-prepared NiFeMn-AOs catalyst shows excellent electrocatalytic performance for OER, attaining a current density of 10 mA cm^{-2} with a low overpotential of 219 mV and a small Tafel slope of 26 mV dec^{-1}. It also shows excellent stability during a 140-hour test. This catalyst drives a current density of 1 A cm^{-2} with an ultra-low potential of 1.473 V under harsh industrial conditions. Moreover, it exhibits superior HER performance, and reaches 10 mA cm^{-2} with an overpotential of only 19 mV in alkaline electrolyte. The result is one of the best records for the NiFe-based catalyst for HER.

Furthermore, the two-electrode electrolyzer manufactured by NiFeMn-AOs shows outstanding performances on water splitting, achieving 15 mA cm^{-2} at a low voltage of 1.46 V. The current density can reach 500 mA cm^{-2} when the voltage of the electrolytic cell is 2.1 V in 1 M KOH. The fundamental mechanism of Mn doping in the NiFeMn-AOs behind the excellent performance of OER and HER has been studied by density-functional-theory (DFT) calculations. The conclusion drawn from the experimental data and DFT calculation shows that NiFeMn-AOs has both outstanding HER catalytic activity and strong OER activity, which provides a new possibility for industrial application in the future.

Experimental

Chemicals and materials

NiCl$_2$·6H$_2$O, MnSO$_4$·H$_2$O, FeCl$_3$·6H$_2$O and KOH were bought from Aladdin Co., Ltd. HCl (37 wt%) and acetone were purchased from Sinopharm Chemical Reagent. Carbon cloth (W0S1009) was purchased from CeTech. RuO$_2$ (Ru ≥59.5%) was purchased from Leyan. Nafion (D520 5%) was purchased from DuPont. Nickel foam (NF) was supplied by Annuohe New Energy Technology Co., Ltd. All reagents were analytically pure, and used without further purification.

Synthesis of NiFeMn-AOs, NiFe-AOs and Ni/NF electrodes

The NiFeMn-AOs was fabricated on a Ni foam substrate by a one-step chronoamperometry deposition process. Before the deposition, the nickel foam was washed in 3 M HCl solution for 15 min with sonication, and followed by water and acetone washing to remove organics and oxides on the surface, then drying under vacuum at room temperature. Then, the NiFeMn-AOs was *in situ* deposited onto the nickel foam by using a chronoamperometry method. The details of the deposition process are as follows: the treated nickel foam was transferred to an electroplating bath with 50 mL aqueous solution, which contains 1 mmol of MnSO$_4$·H$_2$O, 1 mmol of FeCl$_3$·6H$_2$O, 2 mmol of NiCl$_2$·6H$_2$O. Then, the graphite rod, the cleaned nickel foam and Ag/AgCl were used as anode, cathode and reference electrode, respectively. The electroplating process ran for 600 s with a cathode voltage of −2.5 V at an electrochemical workstation. After electrodeposition, the as-prepared NiFeMn-AOs on nickel foam was cleaned by ethanol and DI water, then dried in a vacuum at room temperature, and the mass load of the catalyst is about 21 mg cm^{-2}.

The NiFe-AOs and Ni/NF electrodes were prepared as reference electrodes by an essentially identical procedure with adjusting the molar ratio of Mn, Ni and Fe metal ions in electrodeposition solution. The overall molar amount of metal ions in the electroplating bath is the same. The Ni/Fe ratio of NiFe-AOs is 2 : 1 and the Ni/NF only with Ni^{2+}. The method of manufacturing the flexible NiFeMn-AOs electrode was made in the same way, except that the nickel foam substrate was replaced by a carbon cloth substrate.

Synthesis of NiFe-layered double hydroxide (NiFe-LDH) electrode

NiFe-LDH was synthesized by a one-step hydrothermal method.[29] In a typical procedure, 0.5 mmol $NiCl_2 \cdot 6H_2O$ and $Fe(NO_3)_3 \cdot 9H_2O$ were dissolved in 30 mL of distilled water. Then, 5 mmol of $CO(NH_2)_2$ was added to adjust the pH of the solution. Then, the solution and foamed nickel substrate were transferred to a 50 ml Teflon-lined stainless-steel jar, and then the jar was kept at 120 °C for 12 hours. After washing with deionized water, the NiFe-LDH was achieved on the nickel foam substrate.

Fabrication of the Pt plate and RuO_2/NF electrodes

The Pt plate electrode was a piece of pure platinum with the size of $10 \times 10 \times 0.5$ mm^3. The RuO_2/NF electrode was prepared by the following procedure. First, 10 mg RuO_2, 0.5 mL ethanol, 0.4 mL purity water and 60 μL Nafion were mixed and ultrasonicated for 20 min to acquire a homogeneous dispersion. Second, a piece of treated NF was dipped into the dispersion, and then dried in air at 60 °C. The mass loading of the RuO_2 catalyst on the nickel foam was controlled at approximately 2 mg cm^{-2}.

Materials analysis

The crystallinity of the prepared electrodes was probed by an X-ray diffractometer (XRD, Rigaku Ultima IV, Cu Kα, λ = 0.154178 nm). The surface topography characteristics of the catalyst, the elemental content and the elemental distribution characteristics of the catalyst were detected by scanning electron microscope (SEM, Zeiss Supra 55) and energy dispersive X-ray detector (EDX). The transmission electron microscopy (TEM) and high-angle annular dark field scanning TEM (HAADF-STEM) measurements were conducted by a FEI Tecnai G2 F20 with an acceleration voltage of 200 kV, and the STEM-EDS point sweep was obtained using an OXFORD X-max 80T with an acceleration voltage of 200 kV. Corresponding valence states of the elements were determined by X-ray photoelectron spectroscopy (XPS, Thermo Fisher Scientific K-Alpha, Al Kα). The Raman spectra of the materials were characterized by Raman spectrometer (Renishaw inVia plus; the laser wavelength is 532 nm).

Computational methods

The surface properties of the NiFeMn-AOs and NiFe-AOs were obtained by density functional theory calculations plus Hubbard-U (DFT+U), which were accomplished with the Perdew–Burke–Ernzerhof (PBE) exchange correlation functional and projector-augmented wave (PAW) pseudopotentials,[30,31] as applied in the Vienna *Ab initio* Simulation Package (VASP) code.[32,33] The energy cut-off was implemented to 400 eV. The Brillouin zone was sampled by a gamma k-mesh of $3 \times 3 \times 1$. On the basis of the experience in the previous study,[34] the effective U–J terms were modified at 6.5 eV, 3.5 eV and 3 eV for Ni, Fe and Mn, respectively. The overall calculations were spin-polarized. The vacuum thickness of larger than 25 Å was constructed to simulate the catalytic process on the surface. The energy of 10^{-4} eV was applied for the energy convergence criterion between two electronic steps. For geometry optimization, the maximum force applied on each atom was less than 0.01 eV Å^{-1}.

Electrochemical analysis

The electrochemical characteristics of the electrocatalytic materials were characterized by electrochemical workstation (Princeton VersaSTAT 3F) by using a traditional three-electrode test system at room temperature. The electrolyte was 1 M KOH. A graphite rod was utilized as the counter electrode and an Ag/AgCl electrode (in saturated KCl) was used for the reference electrode. The electrodes after electrochemical deposition served as the working electrode. The working area was tailored to 0.5×0.5 cm^2. The electrode potential was presented *versus* the reversible hydrogen electrode (RHE). The RHE reference scale was determined by using the following equation:

$$E_{RHE} = E_{Ag/AgCl} + 0.0591 \times pH + E^{\Theta}_{Ag/AgCl}$$

Before the test, the electrode was subjected to 20 cycles of 100 mV s^{-1} scan rate by cyclic voltammetry to activate the electrode material. The OER and HER performances of the electrodes were characterized by linear sweep voltammetry (LSV) at a sweep rate of 1 mV s^{-1} to avoid the possible contribution of the capacitive current. Electrochemical impedance spectroscopy (EIS) was applied to measure the ohmic resistance of the electrocatalytic system. The test frequency range of EIS was 10^5 Hz–0.1 Hz, and the amplitude was 5 mV. The electrode potential was corrected with a value of 95% × R_s through the workstation, where R_s is the ohmic resistance obtained by EIS. The ECSA values of the as-prepared electrodes were calculated from the electrochemical double-layer capacitance (C_{dl}) of the electrode morphology. The C_{dl} values of the electrodes were calculated on the basis of the cyclic voltammetry curves recorded in a non-Faradaic range at various sweep rates (20, 40, 80, 160, 240, 320 and 400 mV s^{-1}), and it was calculated by difference of the current density plot (Δj) against the sweep rate, where the C_{dl} is half of the resulting linear slope. The Tafel slope of the polarization curve was calculated by plotting the overpotential and the logarithm of the current density. The long-term stability of the electrocatalyst was evaluated by chronopotentiometry and multi-step chronopotentiometry. The Faraday efficiencies of HER and OER were calculated by comparing the volumes of oxygen and hydrogen that were collected by the replacement water, and the electricity consumed from water splitting.
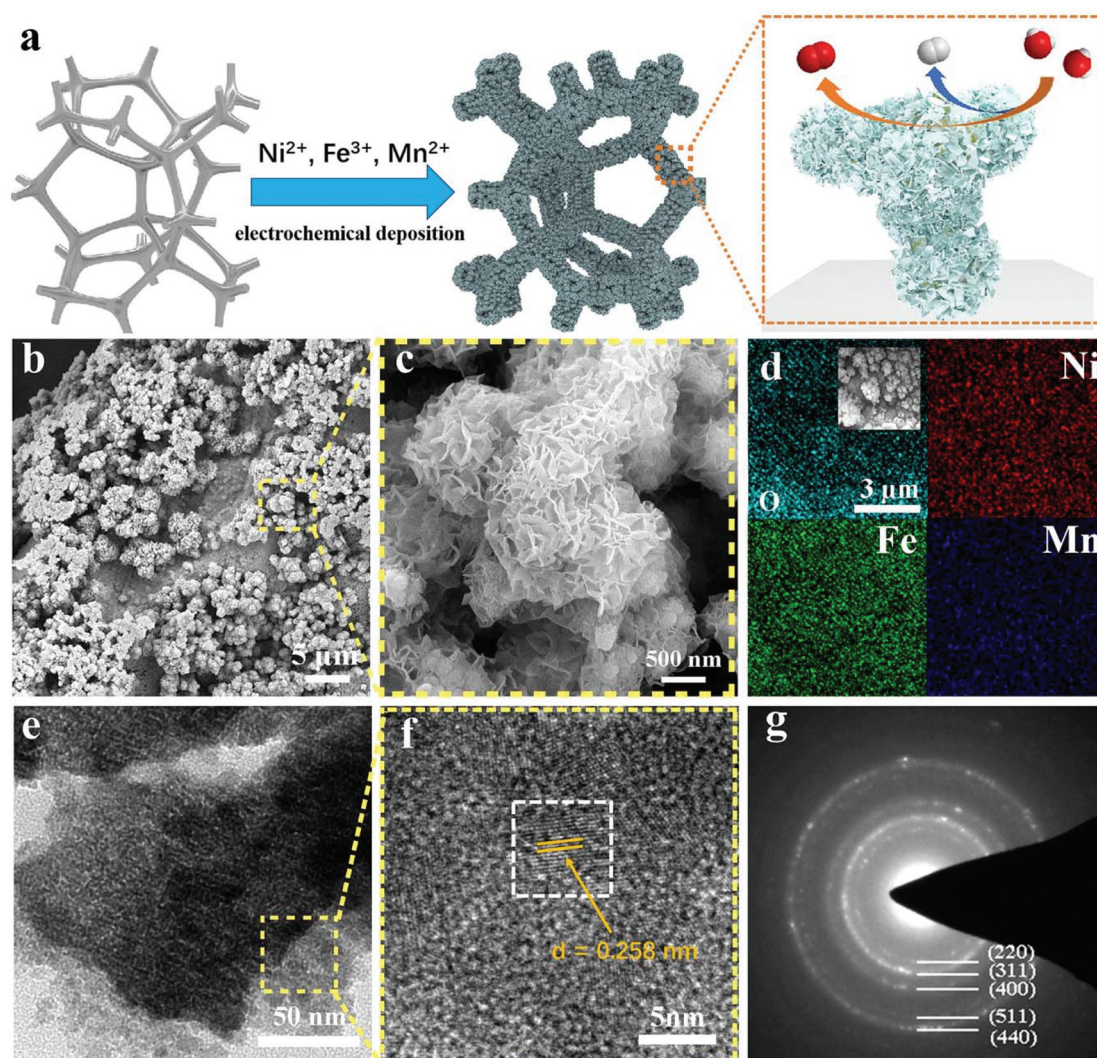
Results and discussion

In this study, the NiFeMn-AOs was prepared by a one-step chronoamperometry electrodeposition method at room temperature, which is a simple method for large-scale application. The high voltage reduced the metal ions to metals, and they attached to the nickel foam substrate to form an alloy skeleton.

This journal is © the Partner Organisations 2021

Inorg. Chem. Front., 2021, **8**, 2713–2724 | **2715**

Then, the metal ions reacted with hydroxide in solution and attached to the electrode surface to form metal oxyhydroxide on the alloy skeleton, thereby forming multi-level dendritic structures (Fig. 1a). To demonstrate the performance of the electrocatalysts, electrodes with diverse metal ratios were fabricated through controlling the molar ratios of nickel, iron and manganese ions in the electrodeposition solution, and named as Ni/NF, NiFe-AOs, NiFeMn-AOs, respectively. All of the samples were deposited on nickel foam. This method can also be deposited on other conductive substrates, such as carbon cloth. We fabricated flexible NiFeMn-AOs on a carbon cloth substrate, which showed good properties with great potential applications for bioelectronic sensors and wearable energy storage devices (see ESI, Fig. S1†).[35,36]

After the NiFeMn-AOs catalyst was synthesized, the surface topography of the electrode was probed by SEM. The SEM images show that (Fig. 1b) a lot of highly porous coral-like structures with sizes from 1 μm to 5 μm are on the NF substrate. At relatively higher magnification, as shown in Fig. 1c, many ultrathin nanosheet architectures are over the coral-like structure, forming a multi-level catalytic system. This revealed that the NiFeMn oxyhydroxide was homogeneously grown on the NiFeMn alloy skeleton. Compared with NiFe-AOs, this structure provides a high surface area with more reactive sites, and also promotes the release of oxygen or hydrogen bubbles from the catalyst (Fig. S2†). The contact angle test demonstrates that the hydrophilicity of the NiFeMn-AOs electrode is significantly improved compared with the foamed nickel (Fig. S3†). These properties are beneficial to the OER and HER process, and it is more obvious under larger current density. In addition, the elemental mapping of EDX illustrated that the multi-level structure is composed of Ni, Fe, Mn and O elements, and they are homogeneously distributed in the electrode (Fig. 1d). The pictures of TEM and HAADF-STEM in

Fig. 1 (a) Schematic illustration of the fabricating process of the NiFeMn-AOs electrode and its catalytic function for both OER and HER. (b and c) SEM images of the NiFeMn-AOs at different magnification. (d) EDX elemental mapping images from SEM. (e) Scanning TEM image of the NiFeMn-AOs. (f and g) HRTEM image of NiFeMn-AOs and corresponding SAED.

2716 | *Inorg. Chem. Front.*, 2021, **8**, 2713–2724

This journal is © the Partner Organisations 2021

Fig. 1e and Fig. S4,† respectively, illustrate that the NiFeMn-AOs is coated with an ultrathin nanosheet array. As shown in the high-resolution TEM (HRTEM) image (Fig. 1f), the nanosheets consist of both nanocrystal and amorphous parts, and the formed lattice spaces of 0.258 nm are attributed to NiFeMn oxides (311). Moreover, the corresponding diffraction rings pattern was obtained by selected area electron diffraction (SAED). They could be assigned to the (220), (311), (400), (511), and (440) planes of the NiFeMn oxides. The NiFeMn oxyhydroxide exhibits a diffuse halo ring between the circles. The above results confirm that the NiFeMn-AOs with multi-layer structure was deposited onto the surface of the nickel foam by the one-step electrodeposition method.

To further analyze the phase composition and crystallinity of NiFeMn-AOs, the XRD pattern was tested, as shown in Fig. S5.† Only the diffraction peak of the NF substrate is found in the patterns of XRD. This result proves that the major structure of NiFeMn-AOs is amorphous. The amorphous structure is usually associated with more reactive sites. After the samples were annealed in a nitrogen atmosphere at 500 °C for two hours (denoted as t-NiFeMn-AOs and t-NiFe-AOs), except for the peaks indexed to NF, two peaks at 29.8° and 35.2° can be indexed to the (220) and (311) planes, respectively, of the cubic structure of $NiFe_2O_4$ (JCPDS no. 74-2081) for the t-NiFe-AOs. Compared with t-NiFe-AOs, the position of the peak of t-NiFeMn-AOs exhibits minor left shifts with the Mn doping, and a new minor peak at 36.7° can be indexed to the (211) plane of MnO_2 (JCPDS no. 44-0141).[37] These results clearly illustrated the successful formation of the NiFeMn oxyhydroxide overlayers on the NiFeMn alloy, and the incorporation of Mn into the electrode.

Furthermore, XPS was applied to detect the major chemical composition and chemical bonding state of the catalyst surface. Specifically, the XPS survey spectrum of the NiFeMn-AOs indicated the coexistence of nickel, iron, magnesium and oxygen elements on the sample surface (Fig. 2a). The high-resolution spectra of Ni 2p (Fig. 2b) show two main peaks corresponding to Ni $2p_{3/2}$ and Ni $2p_{1/2}$, and two minor peaks made up of their satellites peaks (Sat.). Peak fitting indicated the co-existence of Ni^{2+} (855.2, 872.6 eV) and Ni^{3+} (856.3, 873.9 eV), which can be ascribed to $Ni(OH)_2$ and NiOOH, respectively, while two minor peaks (852.5, 869.9 eV) are allocated to Ni^0 (metallic Ni).[38,39] In particular, we noticed that the ratio of the Ni^{3+}/Ni^{2+} peak intensity in NiFeMn-AOs was higher than that of NiFe-AOs. This indicated that there was more NiOOH, which is a key active intermediate with lower OER overpotential.[40] Similarly, the deconvoluted peaks of the Fe 2p spectrum (Fig. 2c) revealed Fe_2O_3 (710.2, 723.7 eV) and FeOOH (713.0,
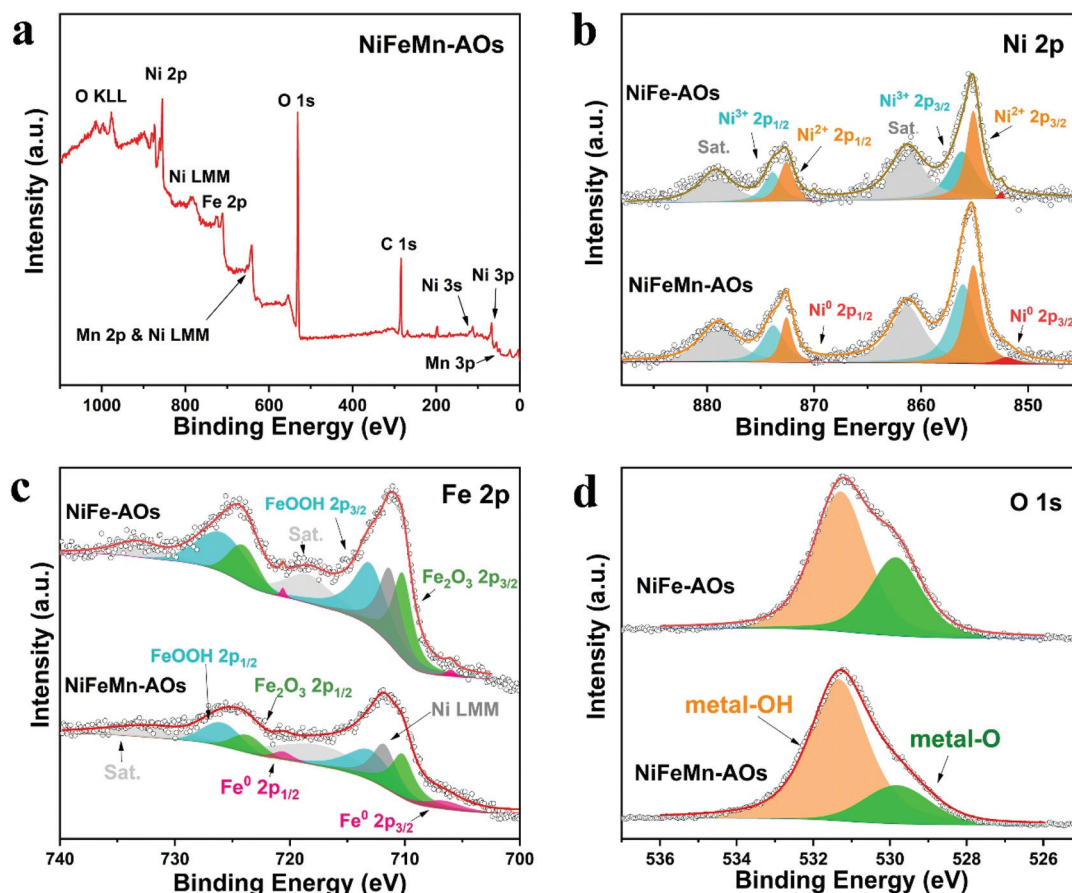

Fig. 2 (a) Wide-scanning XPS survey of the NiFeMn-AOs. (b–d) XPS high-resolution scans of (b) Ni 2p, (c) Fe 2p and (d) O 1s.

This journal is © the Partner Organisations 2021

Inorg. Chem. Front., 2021, **8**, 2713–2724 | **2717**
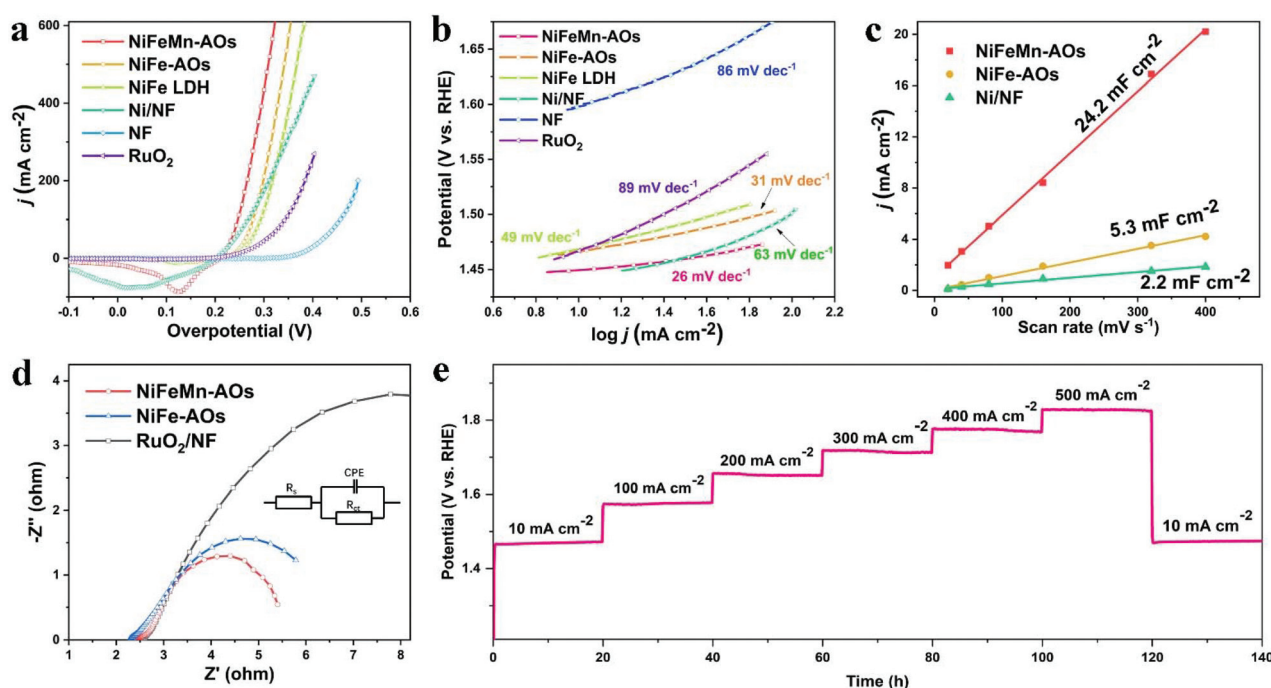
725.9 eV) in the sample, and two minor peaks (706.6, 720.1 eV) are allocated to Fe^0 (metallic Fe). The peak at 711.7 eV can be ascribed to the LMM Auger line of the Ni element, while using Al Kα radiation.[13,41] The Fe_2O_3 on the surface may be generated from $Fe(OH)_3$, which was dehydrated in air and converted to Fe_2O_3. The binding energy of the Fe 2p peaks in NiFeMn-AOs is more positively shifted, and its peak intensity is lower compared with that of the NiFe-AOs. Moreover, compared with the distinct signals of Ni^{3+}/Ni^{2+} and Fe^{3+}, the signal of Ni^0 or Fe^0 is significantly weaker. This phenomenon is due to the deposition of a thin array of amorphous nanosheets on the surface of the electrodes, and it is difficult to detect the photoelectrons generated by the alloy of the skeleton. The high-resolution spectra of Mn 2p are shown in Fig. S6a.† Unfortunately, the peak of Mn $2p_{3/2}$ overlaps with the strong LMM Auger line of the Ni element signals, which makes it difficult to get a precise spectral analysis of the Mn 2p.[42] However, the minor Mn 3p peak at 48 eV in the full spectra indicates the existence of Mn. As shown in Fig. S6b,† two multiple-splitting peaks exist in the Mn 3s spectrum. The binding energy difference between the peaks is 6.3 eV, which reveals that the major valence state of Mn existing in the electrode is Mn^{2+}.[43] The O 1s spectrum exhibited two peaks (529.8, 531.3 eV); they are allocated to metal-O and metal-OH, respectively. Compared with the NiFe-AOs, the NiFeMn-AOs sample shows more metal-OH on the surfaces, which could obviously improve the OER efficiency.[44]

The electrocatalytic properties of the as-prepared NiFeMn-AOs electrode were directly measured by LSV in a three-electrode cell in 1 M KOH electrolyte. The scanning rate was at 1 mV s⁻¹ in order to avoid metal ion redox overlap with the OER polarization curves. For comparison, bare nickel foam, RuO_2/NF, Ni/NF and NiFe-AOs electrodes were also measured. As the OER polarization curves illustrated in Fig. 3a, the state-of-the-art RuO_2/NF shows good OER activity. It required overpotentials of 286 mV and 340 mV to attain current densities of 10 mA cm⁻² and 200 mA cm⁻², respectively. The NF substrate shows hardly any OER activity (370 mV and 493 mV). The NiFeMn-AOs shows the smallest overpotential (219 mV and 268 mV) among all the electrodes we tested. This electrocatalytic activity exceeds the performance of the OER electrocatalysts that have been recently reported (Table S1, ESI†), indicating that the NiFeMn-AOs catalysts could significantly lower the activation energy for the OER reactions. To further evaluate the OER reaction kinetics of these electrocatalysts, the corresponding Tafel analysis was calculated from the LSV curves (Fig. 3b). The Tafel slope value of NiFeMn-AOs is 26 mV dec⁻¹, which is smaller than that of NiFe-AOs (31 mV dec⁻¹), and it is obviously lower than those of Ni/NF (63 mV dec⁻¹), RuO_2 (89 mV dec⁻¹) and foamed nickel (86 mV dec⁻¹), indicating the fast OER reaction kinetics of the NiFeMn-AOs catalyst.

To demonstrate the origin of the intrinsic activity of the different catalysts, the ECSA was determined by measurement of different electrodes conducted at double layer capacitance (C_{dl}). Fig. 3c is based on the cyclic voltammetry curves under different sweep rates, where the current response occurred within the non-Faraday charging potential range of the double layer. The C_{dl} value of the NiFeMn-AOs sample is 24.2 mF

Fig. 3 The performance of the oxygen evolution reaction. (a) The LSV curves of various electrodes. (b) The Tafel plots calculated from polarization curves. (c) C_{dl} values of Ni/NF, NiFe-AOs and NiFeMn-AOs. (d) EIS Nyquist plots of RuO_2/NF, NiFe-AOs and NiFeMn-AOs electrodes with 250 mV overpotential. (e) Multi-chronopotentiometry curves of NiFeMn-AOs under various current densities.
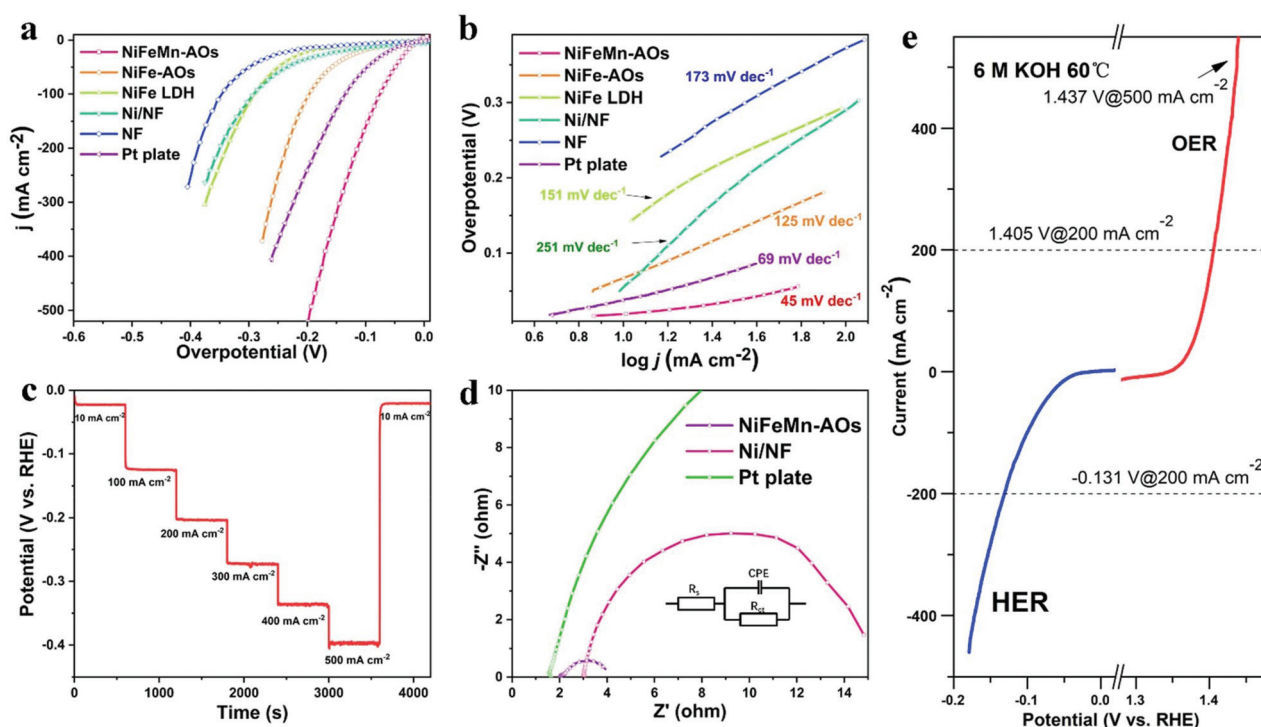
cm^{-2}, which is 4.52 and 11 times larger than the values of the NiFe-AOs and Ni/NF samples, respectively. Generally, the larger C_{dl} suggests larger ECSA and more exposed active sites, which show that the multi-level nanosheet arrays on NiFeMn-AOs are beneficial to get larger surface areas and higher catalytic activity. In addition, we found that it is easier to generate relatively dense NiFe alloys in the electrochemical deposition process if only nickel and iron metal elements are in the electroplating bath, resulting in a smaller ECSA compared to NiFeMn-AOs under the same deposition condition. This phenomenon was more pronounced when only nickel metal elements are electrodeposited. Moreover, the doping of Mn can significantly increase the conductivity of the metal oxyhydroxide, which means that the effective activity of the catalyst is improved.[37,45] From the EIS Nyquist plots in Fig. 3d, the NiFeMn-AOs has a smaller charge-transfer resistance (R_{ct}) (2.72 ohms) compared with RuO$_2$/NF (10.9 ohms) and the NiFe-AOs (3.4 ohms), showing high efficiency in the charge transport and excellent OER dynamics.

The stability of NiFeMn-AOs was also obtained by multi-step chronopotentiometry test in 1 M KOH. As shown in Fig. 3e, the current range is from 10 to 500 mA cm^{-2} for a total of 140 hours (10, 100, 200, 300, 400, 500 and 10 mA cm^{-2} per 20 hours) in the experiment. At the beginning of 10 mA cm^{-2}, the initial value of the potential is at 1.466 V. When the test is completed and the current returns to 10 mA cm^{-2}, the cell potential is 1.474 V, with only 8 mV overpotential increasing.

This result suggests that the NiFeMn-AOs has outstanding mass transportation, mechanical robustness and durability. Moreover, after consecutive 2500 cycles with a sweep rate of 100 mV s^{-1} in the range from 1.2 to 1.5 V, the NiFeMn-AOs still performed efficiently with even a slight increase compared with the initial value. This phenomenon may be due to the alloy on the surface being oxidized to form more active sites (Fig. S7†).[46]

The HER performance of the NiFeMn-AOs catalyst was also measured on a three-electrode cell in 1 M KOH electrolyte. As shown in Fig. 4a, the NiFeMn-AOs reveals outstanding catalytic performance with the ultra-low overpotentials of 19.5 mV and 112.2 mV to attain the current densities of 10 mA cm^{-2} and 200 mA cm^{-2}, respectively. This result is better than that of NiFe-AOs (70.6 mV, 236.4 mV), Pt plate (38.5 mV, 239.8 mV) and NF (140 mV, 389.5 mV). The catalytic ability of the NiFeMn-AOs sample is also one of the strongest non-noble metal catalysts and bi-functional catalysts to be recently reported (Table S2, ESI†). The NiFeMn-AOs exhibit excellent HER activity compared to NiFe-AOs and Pt plate, indicating that the Mn doping is beneficial to increasing the HER catalytic activity.[47] The Tafel slope calculated from the polarization curve are shown in Fig. 4b, the NiFeMn-AOs with a smaller Tafel slope (45 mV dec^{-1}) as compared with Pt plate (69 mV dec^{-1}), the NiFe-AOs (125 mV dec^{-1}) and the pure NF (174 mV dec^{-1}), indicating the NiFeMn-AOs with faster HER reaction kinetics.
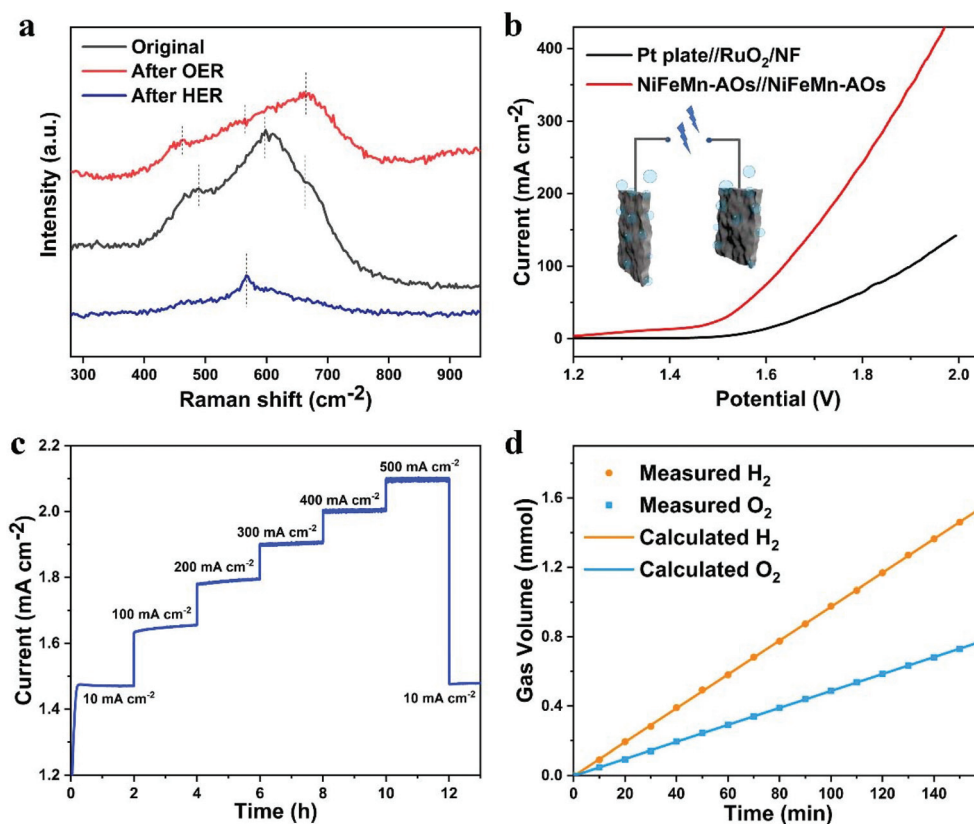

Fig. 4 (a) The LSV curves of various electrodes. (b) The Tafel plots calculated from LSV curves. (c) Multi-chronopotentiometry curves of NiFeMn-AOs at different current densities. (d) EIS Nyquist plots of the Pt plate, Ni/NF and NiFeMn-AOs electrodes with 150 mV overpotential for HER. (e) HER and OER polarization curve of electrode NiFeMn-AOs under industrial operating conditions of 6 M KOH, 60 °C.

This journal is © the Partner Organisations 2021

Inorg. Chem. Front., 2021, **8**, 2713–2724 | **2719**

In addition, the durability of the electrochemical reaction is also a vital factor in assessing the comprehensive performance of the catalyst. The multi-step chronopotentiometry curve of NiFeMn-AOs with seven constant current densities (10, 100, 200, 300, 400, 500 and 10 mA cm^{-2} per 600 s) is shown in Fig. 4c. The overpotential of the sample had a negligible increase after the durability test. Moreover, the NiFeMn-AOs shows a slight activity decay after long-term stability over 50 h by chronopotentiometry measurement (Fig. S8†). These results demonstrate that the NiFeMn-AOs have preeminent HER performance and good stability in an alkaline electrolyte. Similarly, from the EIS Nyquist plots in Fig. 4d, the NiFeMn-AOs has much smaller R_{ct} compared with the Pt plate and Ni/NF, with the smallest R_{ct} value of 1.52 ohms. This result demonstrates that there is faster electron transport kinetics for HER between the interface of the electrolyte and NiFeMn-AOs. Combined with the abovementioned results, doping of Mn by electrodeposition is an effective method for increasing the catalytic performance of HER for NiFeMn-AOs in alkaline electrolyte.

To further understand the catalytic mechanism of the NiFeMn-AOs, the sample was annealed at 500 °C for two hours in the nitrogen atmosphere. The OER and HER performance of the electrode significantly decreased after annealing,

which could be caused by the decrease in ECSA of the electrode after annealing. Furthermore, a relatively low activity of the metal oxides was formed on the surface of the catalyst due to the dehydration of the metal oxyhydroxide (Fig. S9†). Moreover, the catalytic performance of the NiFeMn-AOs electrode was tested under extreme conditions, such as high temperature and concentrated alkaline solution, which are commonly used in commercial alkaline water electrolysers. Fig. 4e and Fig. S10† reveal the OER and HER polarization curves of NiFeMn-AOs in 6 M KOH at 60 °C, respectively. The NiFeMn-AOs electrode shows outstanding activity under harsh industrial conditions. It delivered a current density of 10 mA cm^{-2} and 1 A cm^{-2} at 1.36 V and 1.473 V for OER, respectively. When the cell voltage reached −0.131 V, the current density attained 200 mA cm^{-2} for HER. These results completely satisfy the requirements for commercial water electrolyser applications.

Raman spectroscopy was applied to research the surface of the NiFeMn-AOs before and after OER or HER (Fig. 5a). Three obvious broad peaks can be measured for the original NiFeMn-AOs. The bands at around 488 and 596 cm^{-1} are due to the Ni–O stretching vibrations in the disordered Ni(OH)$_2$ clusters. The frequency of the Ni–O stretching vibrations of the NiFeMn-AOs is higher than that of pure Ni(OH)$_2$, which is due

Fig. 5 (a) Raman spectra of the NiFeMn-AOs sample. (b) Polarization curves of NiFeMn-AOs//NiFeMn-AOs and Pt plate//RuO$_2$ electrolyzer (without iR-compensation). (c) Chronopotentiometry curves of NiFeMn-AOs//NiFeMn-AOs at various current densities. (d) The volumes of H$_2$ and O$_2$ experimentally measured at 100 mA cm^{-2}.
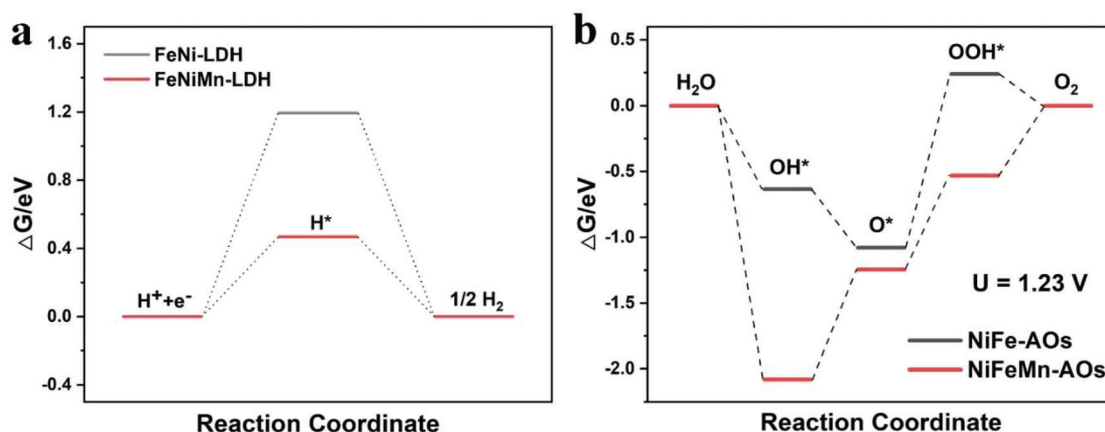
2720 | *Inorg. Chem. Front.*, 2021, **8**, 2713–2724

This journal is © the Partner Organisations 2021

to the insertion of Fe and Mn into the lattice of Ni(OH)$_2$.[41,48] The Raman bands at 662 cm^{-1} may be attributed to the amorphous FeOOH on the electrode.[49] After the process of OER, the peak of Ni(OH)$_2$ shifts to the left and the peak intensity of FeOOH increases significantly, which corresponds to the production of OER catalytically active substances.[50] After HER treatment, most of the oxyhydroxides on NiFeMn-AOs are reduced to metals, so the intensity of the Raman peak is significantly reduced. The minor peak corresponding to Ni(OH)$_2$ appears only at 566 cm^{-1}.[51]

For further development toward industrialized application, it is essential to research the overall water splitting with synergistic converting water to oxygen at the anode and hydrogen at the cathode. Since NiFeMn-AOs exhibits the superior bifunctional performance for OER and HER, an overall water splitting electrolyzer was manufactured through using the NiFeMn-AOs as the anode and also the cathode electrode in 1.0 M KOH electrolyte. The LSV curve of the overall water electrolysis of different samples is presented in Fig. 5b. The NiFeMn-AOs shows the high performance of water electrolysis with a cell voltage of 1.46 V to provide a current density of 15 mA cm^{-2}. This result is superior to the Pt plate//RuO$_2$ (1.59 V), and the bifunctional electrocatalysts that have been recently reported for overall water splitting (Table S3, ESI†). The long-term stability is a key index of the durability of the water electrolyzer. We tested the overall water splitting durability of the NiFeMn-AOs. The result is shown in Fig. 5c. The multi-step chronopotentiometry curve of NiFeMn-AOs had seven constant current densities for a total of 13 hours, and the overpotential has a negligible increase after the test (with only 5 mV). These results indicate that NiFeMn-AOs is a promising non-noble metal catalyst for practical water electrolysis. Moreover, we also measured the polarization curve of the NiFeMn-AOs//NiFeMn-AOs electrolyzer in 6 M KOH at 60 °C and its corresponding durability at 200 mA cm^{-2} (Fig. S11†). The NiFeMn-AOs shows high performance of overall water splitting in commercial alkaline water with an ultra-low voltage of 1.41 V at a current density of

10 mA cm^{-2} and at 1.60 V for 100 mA cm^{-2}, indicating that the NiFeMn-AOs has great potential for industrial application. The faradaic efficiency of this electrolyzer for H$_2$ and O$_2$ generation was also evaluated by water displacement method (Fig. 5d). The proportion of the H$_2$ and O$_2$ volume is close to 2:1. The moles of the collected H$_2$ and O$_2$ are consistent with the result of theoretical calculation by $Q = I \times t$, which showed over 99% faradaic efficiency for the HER and OER processes. Finally, these catalytic results demonstrated that the NiFeMn-AOs have great potential for cosmically commercial applications of hydrogen and oxygen production with low-cost and high performance.

The above experimental measurement results illustrate that with the introduction of Mn into NiFe-AOs, the catalyst could obviously increase the catalytic performance for OER and HER. In order to reveal the essential mechanism of the catalyst performance enhancement (except the increasing of ECSA), DFT was applied to elucidate the OER and HER processes on NiFeMn-AOs. The optimized surface models of NiFeMn-AOs and NiFe-AOs (Fig. S12†) were built on the basis of the NiFe LDH bulk. The calculated adsorbed H* (ΔG_{H*}) values on NiFeMn-AOs and NiFe-AOs are 0.47 and 1.19 eV, respectively (Fig. 6a). The lower value on NiFeMn-AOs elucidates that NiFeMn-AOs is more efficient than NiFe-AOs for the HER process, which is in accordance with the results of the electrochemical experiments. Moreover, the classical four-electron step mechanism was adopted to describe the OER in alkaline electrolyte.[52] Thus, the adsorption energy of OH*, O* and OOH* species on NiFeMn-AOs and NiFe-AOs were calculated (Fig. 6b). The formation of OOH* is the rate-determining step (RDS) on NiFe-AOs with the energy barrier of 1.32 eV at $U = 1.23$ V. However, the RDS becomes the deprotonation of *OH to *O for NiFeMn-AOs with the energy barrier of 0.84 eV, which means that NiFeMn-AOs is more efficient than NiFe-AOs for OER. The above calculations show that the doping of Mn can significantly improve the HER and OER activities of the NiFeMn-AOs catalyst.

Fig. 6 (a) Gibbs free-energy diagram of the HER process of NiFe-AOs and NiFeMn-AOs. (b) Gibbs free-energy diagram of the OER process at 1.23 V for NiFe-AOs and NiFeMn-AOs.

This journal is © the Partner Organisations 2021

Inorg. Chem. Front., 2021, 8, 2713–2724 | 2721

Conclusions

In summary, we have successfully prepared NiFeMn-AOs by electrochemical deposition as a dual-function electrocatalyst for OER and HER. It can be used for the overall water splitting reaction under alkaline conditions. The incorporation of Mn into NiFe-AOs (NiFeMn-AOs) can increase the number of active sites, improve the surface area and change the ratio of different valence states of the elements. These factors ultimately increase the essential activity of the reactive sites. As a consequence, NiFeMn-AOs shows excellent OER performance with an overpotential of 219 mV to deliver a current density of 10 mA cm^{-2} with a Tafel slope of 26 mV dec^{-1} in 1 M KOH, and deliver a current density of 1 A cm^{-2} at an ultra-low potential of 1.473 V under harsh industrial conditions. Moreover, it revealed the excellent HER performances with only 19 mV overpotential to drive a current of 10 mA cm^{-2}. This result is superior to many recently reported NiFe oxides. Meanwhile, when the NiFeMn-AOs two-electrode electrolyzer was tested in 1 M KOH for overall water splitting, it only needed 1.46 V cell voltage to reach 15 mA cm^{-2}, and the current density can reach 500 mA cm^{-2} at a voltage of 2.1 V. The DFT theoretically proves the key role of Mn for the OER and HER performance of NiFeMn-AOs. Theoretically and experimentally, this work demonstrates that NiFeMn-AOs has excellent HER and OER catalytic activity. This study provides an inexpensive and high-performance electrode material for OER and HER, and is also a helpful catalyst manufacturing method for cosmically industrial water splitting in the future.

Author contributions

Zeyu Ge: methodology, investigation, writing original draft. Fei Wang: methodology, investigation. Junji Guo: methodology. Jungang Ma: validation. Chunyan Yu: review. Aihua Zhong: review. Yizhu Xie: supervision, writing – review & editing. All authors discussed and analyzed the data.

Conflicts of interest

There are no conflicts to declare.

Acknowledgements

References

1 S. Chu, Y. Cui and N. Liu, The path towards sustainable energy, *Nat. Mater.*, 2016, **16**, 16–22.

2 X. Zou and Y. Zhang, Noble metal-free hydrogen evolution catalysts for water splitting, *Chem. Soc. Rev.*, 2015, **44**, 5148–5180.

3 W. Chen, H. Wang, Y. Li, Y. Liu, J. Sun, S. Lee, J. S. Lee and Y. Cui, In Situ Electrochemical Oxidation Tuning of Transition Metal Disulfides to Oxides for Enhanced Water Oxidation, *ACS Cent. Sci.*, 2015, **1**, 244–251.

4 B. Zhang, C. Zhu, Z. Wu, E. Stavitski, Y. H. Lui, T. H. Kim, H. Liu, L. Huang, X. Luan, L. Zhou, K. Jiang, W. Huang, S. Hu, H. Wang and J. S. Francisco, Integrating Rh Species with NiFe-Layered Double Hydroxide for Overall Water Splitting, *Nano Lett.*, 2020, **20**, 136–144.

5 Z. P. Wu, X. F. Lu, S. Q. Zang and X. W. Lou, Non–Noble–Metal–Based Electrocatalysts toward the Oxygen Evolution Reaction, *Adv. Funct. Mater.*, 2020, **30**, 1910274.

6 X. Cui, P. Ren, C. Ma, J. Zhao, R. Chen, S. Chen, N. P. Rajan, H. Li, L. Yu, Z. Tian and D. Deng, Robust Interface Ru Centers for High-Performance Acidic Oxygen Evolution, *Adv. Mater.*, 2020, **32**, e1908126.

7 G. Zhao, P. Li, N. Cheng, S. X. Dou and W. Sun, An Ir/Ni (OH)2 Heterostructured Electrocatalyst for the Oxygen Evolution Reaction: Breaking the Scaling Relation, Stabilizing Iridium(V), and Beyond, *Adv. Mater.*, 2020, **32**, e2000872.

8 Y. Jiang, X. Wu, Y. Yan, S. Luo, X. Li, J. Huang, H. Zhang and D. Yang, Coupling PtNi Ultrathin Nanowires with MXenes for Boosting Electrocatalytic Hydrogen Evolution in Both Acidic and Alkaline Solutions, *Small*, 2019, **15**, e1805474.

9 L. Xu, L. L. Cao, W. Xu and Z. H. Pei, One-step electrosynthesis of NiFe-NF electrodes for highly efficient overall water splitting, *Appl. Surf. Sci.*, 2020, **503**, 144122.

10 B. C. Qiu, L. J. Cai, Y. Wang, Z. Y. Lin, Y. P. Zuo, M. Y. Wang and Y. Chai, Fabrication of Nickel-Cobalt Bimetal Phosphide Nanocages for Enhanced Oxygen Evolution Catalysis, *Adv. Funct. Mater.*, 2018, **28**, 1706008.

11 L. Yu, Q. Zhu, S. Song, B. McElhenny, D. Wang, C. Wu, Z. Qin, J. Bao, Y. Yu, S. Chen and Z. Ren, Non-noble metal-nitride based electrocatalysts for high-performance alkaline seawater electrolysis, *Nat. Commun.*, 2019, **10**, 5106.

12 X. Zheng, X. Han, Y. Cao, Y. Zhang, D. Nordlund, J. Wang, S. Chou, H. Liu, L. Li, C. Zhong, Y. Deng and W. Hu, Identifying Dense NiSe2 /CoSe2 Heterointerfaces Coupled with Surface High-Valence Bimetallic Sites for Synergistically Enhanced Oxygen Electrocatalysis, *Adv. Mater.*, 2020, **32**, e2000607.

13 Y. Teng, X. D. Wang, J. F. Liao, W. G. Li, H. Y. Chen, Y. J. Dong and D. B. Kuang, Atomically Thin Defect-Rich Fe-Mn-O Hybrid Nanosheets as High Efficient Electrocatalyst for Water Oxidation, *Adv. Funct. Mater.*, 2018, **28**, 1802463.

14 B.-J. Kim, X. Cheng, D. F. Abbott, E. Fabbri, F. Bozza, T. Graule, I. E. Castelli, L. Wiles, N. Danilovic, K. E. Ayers, N. Marzari and T. J. Schmidt, Highly Active Nanoperovskite Catalysts for Oxygen Evolution Reaction: Insights into

Activity and Stability of Ba0.5Sr0.5Co0.8Fe0.2O2+δ and PrBaCo$_2$O5+δ, *Adv. Funct. Mater.*, 2018, **28**, 1804355.

15 L. Lei, D. L. Huang, C. Y. Zhou, S. Chen, X. L. Yan, Z. H. Li and W. J. Wang, Demystifying the active roles of NiFe-based oxides/(oxy)hydroxides for electrochemical water splitting under alkaline conditions, *Coord. Chem. Rev.*, 2020, **408**, 213177.

16 C. L. Xiao, Y. B. Li, X. Y. Lu and C. Zhao, Bifunctional Porous NiFe/NiCo$_2$O4/Ni Foam Electrodes with Triple Hierarchy and Double Synergies for Efficient Whole Cell Water Splitting, *Adv. Funct. Mater.*, 2016, **26**, 3515–3523.

17 L. Trotochaud, S. L. Young, J. K. Ranney and S. W. Boettcher, Nickel-iron oxyhydroxide oxygen-evolution electrocatalysts: the role of intentional and incidental iron incorporation, *J. Am. Chem. Soc.*, 2014, **136**, 6744–6753.

18 M. Gong, Y. Li, H. Wang, Y. Liang, J. Z. Wu, J. Zhou, J. Wang, T. Regier, F. Wei and H. Dai, An advanced Ni-Fe layered double hydroxide electrocatalyst for water oxidation, *J. Am. Chem. Soc.*, 2013, **135**, 8452–8455.

19 K. Zhu, J. Chen, W. Wang, J. Liao, J. Dong, M. O. L. Chee, N. Wang, P. Dong, P. M. Ajayan, S. Gao, J. Shen and M. Ye, Etching–Doping Sedimentation Equilibrium Strategy: Accelerating Kinetics on Hollow Rh–Doped CoFe–Layered Double Hydroxides for Water Splitting, *Adv. Funct. Mater.*, 2020, **30**, 2003556.

20 H. F. Fan, W. Chen, G. L. Chen, J. Huang, C. S. Song, Y. Du, C. R. Li and K. Ostrikov, Plasma-heteroatom-doped Ni-V-Fe trimetallic phospho-nitride as high-performance bifunctional electrocatalyst, *Appl. Catal., B*, 2020, **268**, 118440.

21 L. Huang, D. Chen, G. Luo, Y. R. Lu, C. Chen, Y. Zou, C. L. Dong, Y. Li and S. Wang, Zirconium-Regulation-Induced Bifunctionality in 3D Cobalt-Iron Oxide Nanosheets for Overall Water Splitting, *Adv. Mater.*, 2019, **31**, e1901439.

22 R. Subbaraman, D. Tripkovic, K. C. Chang, D. Strmcnik, A. P. Paulikas, P. Hirunsit, M. Chan, J. Greeley, V. Stamenkovic and N. M. Markovic, Trends in activity for the water electrolyser reactions on 3d M(Ni,Co,Fe,Mn) hydr(oxy)oxide catalysts, *Nat. Mater.*, 2012, **11**, 550–557.

23 S. Park, Y. H. Lee, S. Choi, H. Seo, M. Y. Lee, M. Balamurugan and K. T. Nam, Manganese oxide-based heterogeneous electrocatalysts for water oxidation, *Energy Environ. Sci.*, 2020, **13**, 2310–2340.

24 M. Carmo, D. L. Fritz, J. Merge and D. Stolten, A comprehensive review on PEM water electrolysis, *Int. J. Hydrogen Energy*, 2013, **38**, 4901–4934.

25 X. P. Wang, H. J. Wu, S. B. Xi, W. S. V. Lee, J. Zhang, Z. H. Wu, J. O. Wang, T. D. Hu, L. M. Liu, Y. Han, S. W. Chee, S. C. Ning, U. Mirsaidov, Z. B. Wang, Y. W. Zhang, A. Borgna, J. Wang, Y. H. Du, Z. G. Yu, S. J. Pennycook and J. M. Xue, Strain stabilized nickel hydroxide nanoribbons for efficient water splitting, *Energy Environ. Sci.*, 2020, **13**, 229–237.

26 J. Zhu, M. Xiao, G. Li, S. Li, J. Zhang, G. Liu, L. Ma, T. Wu, J. Lu, A. Yu, D. Su, H. Jin, S. Wang and Z. Chen, A Triphasic Bifunctional Oxygen Electrocatalyst with Tunable and

27 Y. Duan, Z. Y. Yu, S. J. Hu, X. S. Zheng, C. T. Zhang, H. H. Ding, B. C. Hu, Q. Q. Fu, Z. L. Yu, X. Zheng, J. F. Zhu, M. R. Gao and S. H. Yu, Scaled-Up Synthesis of Amorphous NiFeMo Oxides and Their Rapid Surface Reconstruction for Superior Oxygen Evolution Catalysis, *Angew. Chem., Int. Ed.*, 2019, **58**, 15772–15777.

28 S. Shetty, M. M. J. Sadiq, D. K. Bhat and A. C. Hegde, Electrodeposition and characterization of Ni-Mo alloy as an electrocatalyst for alkaline water electrolysis, *J. Electroanal. Chem.*, 2017, **796**, 57–65.

29 Z. Lu, W. Xu, W. Zhu, Q. Yang, X. Lei, J. Liu, Y. Li, X. Sun and X. Duan, Three-dimensional NiFe layered double hydroxide film for high-efficiency oxygen evolution reaction, *Chem. Commun.*, 2014, **50**, 6479–6482.

30 J. P. Perdew, K. Burke and M. Ernzerhof, Generalized Gradient Approximation Made Simple, *Phys. Rev. Lett.*, 1996, **77**, 3865–3868.

31 P. E. Blochl, Projector augmented-wave method, *Phys. Rev. B: Condens. Matter Mater. Phys.*, 1994, **50**, 17953–17979.

32 G. Kresse and J. Furthmuller, Efficiency of *ab initio* total energy calculations for metals and semiconductors using a plane-wave basis set, *Comput. Mater. Sci.*, 1996, **6**, 15–50.

33 G. Kresse and J. Furthmuller, Efficient iterative schemes for ab initio total-energy calculations using a plane-wave basis set, *Phys. Rev. B: Condens. Matter Mater. Phys.*, 1996, **54**, 11169–11186.

34 J. Zhang, J. Liu, L. Xi, Y. Yu, N. Chen, S. Sun, W. Wang, K. M. Lange and B. Zhang, Single-Atom Au/NiFe Layered Double Hydroxide Electrocatalyst: Probing the Origin of Activity for Oxygen Evolution Reaction, *J. Am. Chem. Soc.*, 2018, **140**, 3876–3879.

35 A. Sahasrabudhe, H. Dixit, R. Majee and S. Bhattacharyya, Value added transformation of ubiquitous substrates into highly efficient and flexible electrodes for water splitting, *Nat. Commun.*, 2018, **9**, 2014.

36 Y. Z. Xie, Y. Liu, Y. D. Zhao, Y. H. Tsang, S. P. Lau, H. T. Huang and Y. Chai, Stretchable all-solid-state supercapacitor with wavy shaped polyaniline/graphene electrode, *J. Mater. Chem. A*, 2014, **2**, 9142–9149.

37 D. M. Morales, M. A. Kazakova, S. Dieckhöfer, A. G. Selyutin, G. V. Golubtsov, W. Schuhmann and J. Masa, Trimetallic Mn–Fe–Ni Oxide Nanoparticles Supported on Multi–Walled Carbon Nanotubes as High–Performance Bifunctional ORR/OER Electrocatalyst in Alkaline Media, *Adv. Funct. Mater.*, 2019, **30**, 1905992.

38 H. D. Yang, Y. Liu, S. Luo, Z. M. Zhao, X. Wang, Y. T. Luo, Z. X. Wang, J. Jin and J. T. Ma, Lateral-Size-Mediated Efficient Oxygen Evolution Reaction: Insights into the Atomically Thin Quantum Dot Structure of NiFe2O4, *ACS Catal.*, 2017, **7**, 5557–5567.

39 Y. Zhao, X. Jia, G. Chen, L. Shang, G. I. Waterhouse, L. Z. Wu, C. H. Tung, D. O'Hare and T. Zhang, Ultrafine NiO Nanosheets Stabilized by TiO2 from Monolayer NiTi-

This journal is © the Partner Organisations 2021

Inorg. Chem. Front., 2021, **8**, 2713–2724 | **2723**

LDH Precursors: An Active Water Oxidation Electrocatalyst, *J. Am. Chem. Soc.*, 2016, **138**, 6517–6524.

40 A. Govind Rajan, J. M. P. Martirez and E. A. Carter, Facet-Independent Oxygen Evolution Activity of Pure beta-NiOOH: Different Chemistries Leading to Similar Overpotentials, *J. Am. Chem. Soc.*, 2020, **142**, 3600–3612.

41 C. Liang, P. Zou, A. Nairan, Y. Zhang, J. Liu, K. Liu, S. Hu, F. Kang, H. J. Fan and C. Yang, Exceptional performance of hierarchical Ni–Fe oxyhydroxide@NiFe alloy nanowire array electrocatalysts for large current density water splitting, *Energy Environ. Sci.*, 2020, **13**, 86–95.

42 M. Fang, D. Han, W. B. Xu, Y. Shen, Y. M. Lu, P. J. Cao, S. Han, W. Y. Xu, D. L. Zhu, W. J. Liu and J. C. Ho, Surface-Guided Formation of Amorphous Mixed-Metal Oxyhydroxides on Ultrathin MnO_2 Nanosheet Arrays for Efficient Electrocatalytic Oxygen Evolution, *Adv. Energy Mater.*, 2020, **10**, 2001059.

43 E. S. Ilton, J. E. Post, P. J. Heaney, F. T. Ling and S. N. Kerisit, XPS determination of Mn oxidation states in Mn (hydr)oxides, *Appl. Surf. Sci.*, 2016, **366**, 475–485.

44 Y. K. Li, G. Zhang, W. T. Lu and F. F. Cao, Amorphous Ni-Fe-Mo Suboxides Coupled with Ni Network as Porous Nanoplate Array on Nickel Foam: A Highly Efficient and Durable Bifunctional Electrode for Overall Water Splitting, *Adv. Sci.*, 2020, **7**, 1902034.

45 Z. Lu, L. Qian, Y. Tian, Y. Li, X. Sun and X. Duan, Ternary NiFeMn layered double hydroxides as highly-efficient oxygen evolution catalysts, *Chem. Commun.*, 2016, **52**, 908–911.

46 Y. Huang, Z. H. Xu, J. Q. Mai, T. K. Lau, X. H. Lu, Y. J. Hsu, Y. S. Chen, A. C. H. Lee, Y. L. Hou, Y. S. Meng and Q. Li, Revisiting the origin of cycling enhanced capacity of Fe3O4 based nanostructured electrode for lithium ion batteries, *Nano Energy*, 2017, **41**, 426–433.

47 Q. Shao, Y. Wang, S. Yang, K. Lu, Y. Zhang, C. Tang, J. Song, Y. Feng, L. Xiong, Y. Peng, Y. Li, H. L. Xin and X. Huang, Stabilizing and Activating Metastable Nickel Nanocrystals for Highly Efficient Hydrogen Evolution Electrocatalysis, *ACS Nano*, 2018, **12**, 11625–11631.

48 Z. Qiu, Y. Ma and T. Edvinsson, In operando Raman investigation of Fe doping influence on catalytic NiO intermediates for enhanced overall water splitting, *Nano Energy*, 2019, **66**, 104118.

49 B. J. Trzesniewski, O. Diaz-Morales, D. A. Vermaas, A. Longo, W. Bras, M. T. Koper and W. A. Smith, In Situ Observation of Active Oxygen Species in Fe-Containing Ni-Based Oxygen Evolution Catalysts: The Effect of pH on Electrochemical Activity, *J. Am. Chem. Soc.*, 2015, **137**, 15112–15121.

50 J. M. P. Martirez and E. A. Carter, Unraveling Oxygen Evolution on Iron-Doped beta-Nickel Oxyhydroxide: The Key Role of Highly Active Molecular-like Sites, *J. Am. Chem. Soc.*, 2019, **141**, 693–705.

51 M. Ferrandon, J. Carno, S. Jaras and E. Bjornbom, Total oxidation catalysts based on manganese or copper oxides and platinum or palladium I: Characterisation, *Appl. Catal., A*, 1999, **180**, 141–151.

52 D. Friebel, M. W. Louie, M. Bajdich, K. E. Sanwald, Y. Cai, A. M. Wise, M. J. Cheng, D. Sokaras, T. C. Weng, R. Alonso-Mori, R. C. Davis, J. R. Bargar, J. K. Norskov, A. Nilsson and A. T. Bell, Identification of highly active Fe sites in (Ni,Fe) OOH for electrocatalytic water splitting, *J. Am. Chem. Soc.*, 2015, **137**, 1305–1313.